Multiple Zonal Flow Regimes in a Two-Layer Model (Extended Abstract)

Tôhoku Geophys. Journ. (Sci. Rep. Tôhoku Univ., Ser. 5), Vol. 36, No. 2, pp. 200-206, 2001

Multiple Zonal Flow Regimes in a Two-Layer Model (Extended Abstract)

HITOSHI MUKOUGAWA and MUTSUMI ABE

Graduate School of Environmental Earth Science, Hokkaido University,
North-10, West-5, Kita-ku, Sapporo, 060-0810

(Received October 30, 2000)

1. Introduction

Observational studies (*e.g.* Yoden *et al.*, 1987 ; Hartman and Lo, 1998) have revealed that the tropospheric zonal wind variation in the southern hemisphere is recognized as an irregular transition between single and double jet structures. By conducting simplified GCM experiments, Yu and Hartmann (1993) and Akahori and Yoden (1997) indicated that this dominant annular (or zonally symmetric) variability results from nonlinear interaction between zonal flow and synoptic scale baroclinic eddies. Recently, Itoh *et al.* (1999) also suggested that the alternation between these two zonal flow structures can be understood in the framework of the chaotic wandering between flow regimes by examining the bifurcation of chaotic solutions in a 7-level global primitive model. However, since the model used in their study is still complicated, the existence of chaotic attractors, which are necessary to justify this viewpoint of chaotic wandering, has not been shown clearly.

In this study, by using a two-layer quasi-geostrophic model, we will pursue the dynamical basis of the alternation between single and double jet structures in the context of the multiple zonal flow regimes, and try to reveal the role of baroclinic eddies in the maintenance and transition of the zonal flow regime. We also have to notice that there are several works on the zonal flow variability in simple mechanistic models, such as Lee and Feldstein (1996), but they have examined meridional wandering of single jet structure, but the transition between single and double jet structures has not been investigated.

2. Model Description

A two-layer quasi-geostrophic β-channel model is used. The model includes an external thermal forcing representing the differential solar heating between the equator and pole. The vorticity and thermodynamic equations are given by

$$\frac{\partial}{\partial t}\nabla^2\psi_l = -\mathrm{J}(\psi_l, \nabla\psi_l + \beta y) + \frac{f_0}{\Delta p}(\omega_{l+1/2} - \omega_{l-1/2}) - h\nabla^6\psi_l, \qquad (l=1, 2), \tag{1}$$

$$\frac{\partial}{\partial t}(\psi_1 - \psi_2) = -\frac{1}{2}\mathrm{J}(\psi_1 + \psi_2, \psi_1 - \psi_2) + \frac{S\Delta p}{f_0}\omega_{3/2} + \mu\{2\theta^* - (\psi_1 - \psi_2)\}, \tag{2}$$

where subscripts 1 and 2 indicate the upper and lower layers, 1/2, 3/2, and 5/2 the top, middle, and bottom of the model, respectively. Here, ψ is the geostrophic streamfunction ; ω the vertical p-velocity ; J the Jacobian ; $f=f_0+\beta y$ the Coriolis parameter ; Δp the pressure difference between

model levels; S a measure of static stability; h a coefficient of subgrid damping; μ a coefficient of Newtonian cooling; θ^* is an imposed external thermal forcing.

A cyclic boundary condition is assumed at $x=0$ and $x=2\pi L/a$, and two rigid walls are placed at $y=0$ and $y=\pi L$. Thus, the aspect ratio of this channel model is $2/a$. The upper boundary condition is given by $\omega_{1/2}=0$. As a lower boundary condition representing the Ekman friction, we adopt $\omega_{5/2}=-k\Delta p\nabla^2\psi_2/f_0$, where k is a coefficient of Ekman damping.

The dependent variables in (1) and (2) are expanded in the following truncated orthonormal functions which satisfy the imposed horizontal boundary conditions:

$$\begin{cases} F_{A_m}=\sqrt{2}\cos m(y/L), \\ F_{K^n_m}=2\sin m(y/L)\cos na(x/L), \\ F_{L^n_m}=2\sin m(y/L)\sin na(x/L), \end{cases} \tag{3}$$

where $m=1, 2, \ldots, M$ and $n=1, 2, \ldots, N$. The adopted truncation wavenumber is $N=M=21$; This model resolution is fine enough to represent baroclinic waves.

The external thermal forcing is assumed to have the meridional profile,

$$\theta^*=\sqrt{2}\theta^*_{A_1}\cos(y/L)=\sqrt{2}\theta^*_A\cos(y/L), \tag{4}$$

which represents the differential heating between the equator and pole, and we change the strength of the forcing θ^*_A as a bifurcation parameter.

Although we have conducted several numerical experiments by changing the size of the channel, in this report, we will present the results of a case where clear transition between single and double jet structures is observed. In this case, the channel is placed at 45°N with the meridional width of 90 degrees, and the zonal extent of the channel corresponds to the planetary zonal wavenumber 2 in the latitude circle at 45°N. The parameter values are $L=3.19\times10^6$ m, $a=\sqrt{2}$, $f_0=1.03\times10^{-4}\mathrm{s}^{-1}$, $\beta=1.61\times10^{-11}\mathrm{m}^{-1}\mathrm{s}^{-1}$, $S=30$ K/500 hPa, $\Delta p=500$ hPa, $1/k=10$ days, $1/\mu=30$ days, $1/h=6$ hrs. at $M=N=21$. Time integration is made by 4-th order Runge-Kutta method from several initial conditions, and we analyze sets of twice-daily data during 20,000 days after an initial transient period.

3. Results

a. Bifurcation of solutions

The bifurcation of solutions in the model is examined by changing the parameter θ^*_A from 0.0 to 0.05 (the corresponding temperature difference across the channel is from 0 to 105 K). The model has a stationary solution without wave component independent of θ^*_A. However, this solution becomes baroclinically unstable for $\theta^*_A\geq0.013$. A stable periodic solution bifurcates from this Hopf bifurcation point. For $\theta^*_A\geq0.015$\$, the periodic solution bifurcates into aperiodic solutions of which zonal-mean zonal wind structure distinctively depends on the forcing θ^*_A.

Figure 1 shows the bifurcation diagram of chaotic attractors, in which the attractor is characterized by the meridional temperature difference between two walls. For $0.015\leq\theta^*_A\leq0.026$, a chaotic solution [**C** (center)-Jet attractor] which has a persistent single jet structure in the center of the channel exists. For $0.024\leq\theta^*_A\leq0.029$, we obtain another chaotic attractor [**D**(double)-Jet attractor] associated with persistent double jets structure. The time variation of the barotropic zonal wind in **D**-Jet attractor is shown in Fig. 2a. These two attractor coexists

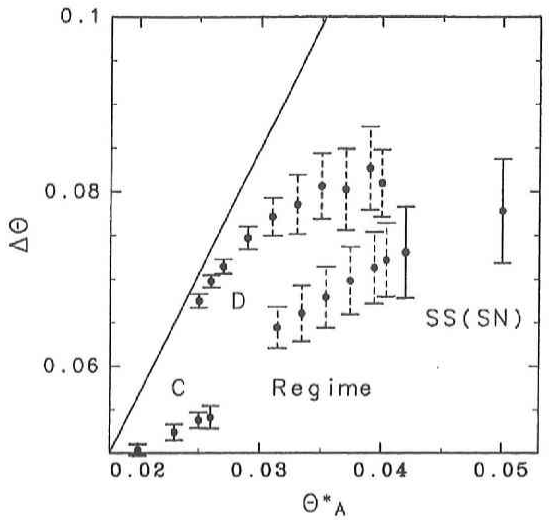

Fig. 1. Bifurcation diagram of chaotic attractor for the external parameter θ_A^*. The ordinate denotes the meridional temperature difference between two walls ($\Delta\theta$). The straight line corresponds to the stationary solution (radiative equilibrium). The time mean value and standard deviation of $\Delta\theta$ for each attractor and regime are indicated by dot and error bar, respectively. Dotted error bars correspond to zonal flow regimes.

for $0.024 \leq \theta_A^* \leq 0.026$. For $\theta_A^* \geq 0.042$, we obtain two other chaotic attractors. Each attractor is characterized by a westerly jet located in the southern or northern half of the channel, and we call it **SS**(Single South)-Jet attractor (Fig. 2b) and **SN**(Singe North)-Jet attractor (Fig. 2c), respectively. The multiplicity of these attractors results from a spatial symmetry in this channel model. From Fig. 1, we also find that the equilibrated temperature difference in the chaotic solution is quite small compared with that of the stationary solution (straight line), especially for large forcing values. This is due to northward heat flux by energetic baroclinic eddies. Moreover, the multiplicity of nonlinear baroclinic adjustment is also noticed, which is associated with the multiplicity of **C**- and **D**-Jet attractors.

b. Multiple zonal flow regimes

Now, we are going to examine the intermediate range of the forcing, $0.029 < \theta_A^* < 0.042$. Figure 3 shows the time variation of barotropic zonal-mean zonal wind for $\theta_A^* = 0.035$. We can easily recognize that the meridional jet structure makes an spontaneous transition among double jet regime, single south jet regime and single north jet regime. Each zonal flow regime becomes a stable chaotic attractor in the adjacent parameter ranges (Fig. 1).

In order to examine the statistics and dynamics of each flow regime, we define each regime event by the following way. At first, we compute the "distance" from the centroid of each chaotic attractor at $\theta_A^* = 0.029$ and 0.042 (Fig. 4). The distance is measured by the barotropic zonal flow components. Then, each regime event is defined when the distance is smaller than a specified threshold value. Here, we tentatively use the standard deviation of the distance in **SS**-Jet attractor (horizontal line in Fig. 4), of which variability is much larger than that in **D**-Jet attractor.

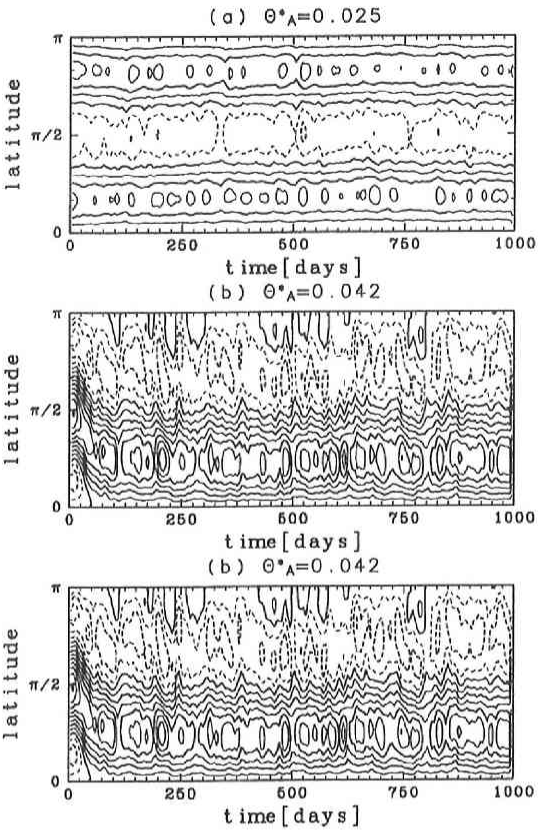

Fig. 2. Time-latitude section of the barotropic zonal-mean zonal wind for (a) D-Jet, (b) SS-Jet, and (c) SN-Jet attractors. An 11-day running average is applied. Solid contours are positive, dashed contours are negative. Contour interval is 0.025.

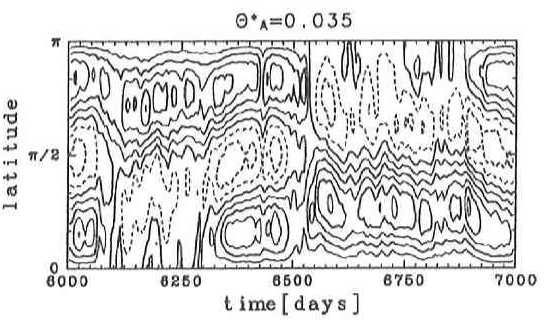

Fig. 3. As in Fig. 2 but for $\theta_A^*=0.035$.

By using this definition of the zonal flow regime, meridional temperature difference in each regime can be shown in Fig. 1. Each zonal flow regime is smoothly connected with the chaotic attractor. Thus, the multiple zonal flow regime in this model can be understood as the chaotic wandering among ruin attractors. This behavior is called the chaotic itinerancy in the context of the nonlinear dynamics.

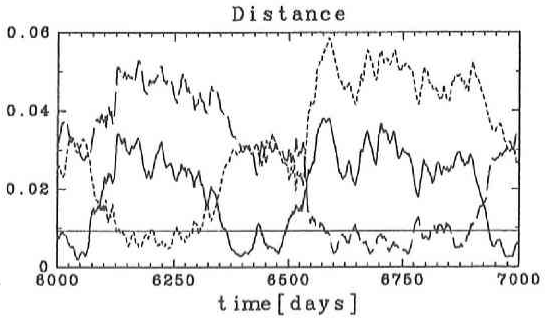

Fig. 4. Time variation of "distance" from D-Jet attractor (solid line), SS-Jet attractor (broken line) and SN-Jet attractor (dotted line). An 11-day running average is applied. Horizontal thin line denotes the threshold value to define each regime event.

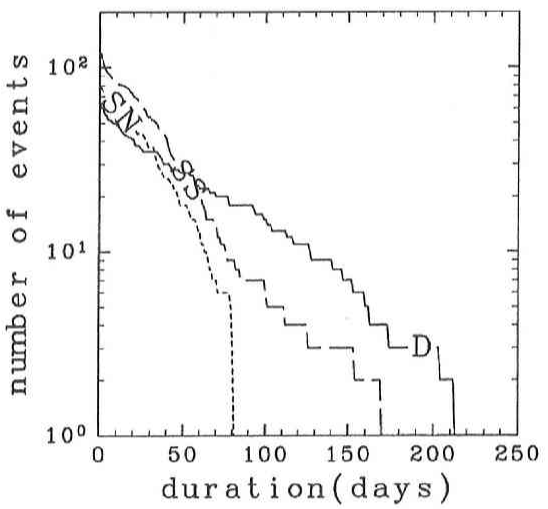

Fig. 5. Persistence distribution of D-Jet regime (solid line), SS-Jet regime (broken line), SN-Jet regime (dotted line) at $\theta_A^*=0.035$. The ordinate is the total number of events which persist over n days on a log-scale, and the abscissa is in days.

Persistence characteristic of each zonal flow regime is shown by Fig. 5, in which the number of regime events persisting over n days at $\theta_A^*=0.035$ is plotted against duration. These lines are well represented by the exponential function. Thus, the probability of one regime event that persisted n days to persist another day is almost independent of its duration, which means that there is no signs of preferred duration in the zonal flow regime.

Figure 6 shows the energy conversion rate from the zonal kinetic energy to the eddy kinetic energy for each zonal flow regime at different thermal forcing values. In the average sense, the time mean value, which is denoted by dots in this figure, has a negative value. Thus, the jet structure of each regime is maintained by the barotropic energy conversion of baroclinic eddies. However, the variance, which is indicated by the error bars in this figure, is so large that its sign becomes positive during regime events. This means that the meridional distribution of eddy momentum flux is very sensitive to the jet structure. Although we also examined other energy

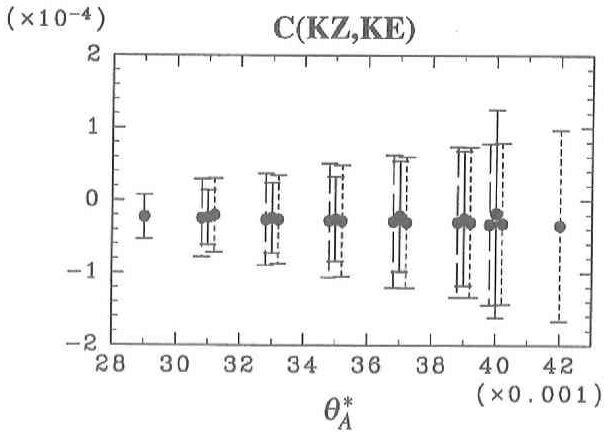

Fig. 6. Energy conversion rate from the zonal kinetic energy to the eddy kinetic energy during D-Jet regime (solid line), SS-Jet regime (broken line), SN-Jet regime (dotted line). The time mean value and standard deviation for each regime are indicated by dot and error bar, respectively.

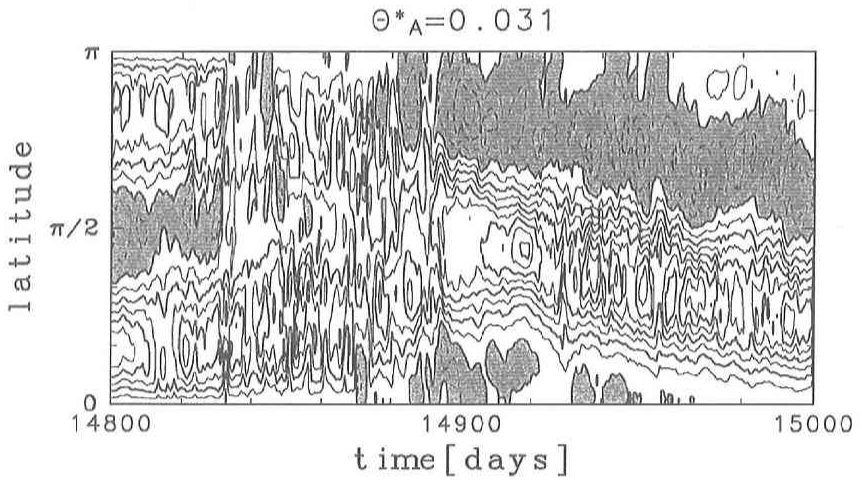

Fig. 7. As in Fig. 2 but for $\theta_A^*=0.031$. Negative values are shaded.

conversion terms, each energy conversion rate has no significant difference between zonal flow regimes.

c. Transition between zonal flow regimes

Finally, we investigate the transition between zonal flow regimes. In order to simplify the analysis, we examine the model behavior at $\theta_A^*=0.031$, where the transition proceeds slowly in time. Figure 7 shows the time sequence of the barotropic zonal-mean zonal wind over 200 days. This period corresponds to the break of a **D**-Jet regime event and the onset of a **SS**-Jet regime event. The break of the double jet structure around day 14,830 is induced by the abrupt enhancement of the potential vorticity (PV) flux (not shown). This is accompanied with the wave breaking of baroclinic eddies. After that, the meridional mixing of PV is enhanced and two jet

axes gradually shift to the center of the channel and a single jet is formed in the center of the channel (around day 14,890). The westerly jet is then gradually strengthened by the convergence of momentum flux by weak baroclinic eddies. However, after an abrupt change of the wave structure around day 14,920, the jet gradually shifts to the south by the wave breaking in the northern flank of the westerly jet. This leads to the onset of a **SS**-Jet regime event (day 14,970). Finally, diabatic heating gradually creates a westerly jet near the north wall and builds up the next **D**-Jet regime.

4. Concluding Remarks

In order to reveal zonal flow variations in a two-layer model in the context of the multiple zonal flow regimes, we have conducted several numerical experiments and obtained the following results. (1) The multiple zonal flow regimes in this model are understood as chaotic wandering among ruin attractors. (2) Multiple zonal flow regimes are characterized by the transition between single and double jet structures, and each regime is maintained by baroclinic eddies in the average sense. However, there is no significant difference in the energetics of each regime. (3) There are two elements in the transition mechanism : One is a fast process associated with the meridional PV mixing due to breaking baroclinic eddies ; The other is a slow process in which diabatic heating gradually builds up jet structure.

Finally, we have to notice that the meridional profile of momentum flux due to baroclinic eddies is very sensitive to the jet structure, especially in the transition periods. Thus, the further investigation on this sensitivity is necessary to understand the maintenance and transition mechanism of the zonal flow regime.

Acknowledgements : The GFD-DENNOU Library was used to draft the figures.

References

Akahori, K. and S. Yoden, 1997 : Zonal flow vacillation and bimodality of baroclinic eddy life cycles in a simple global circulation model, *J. Atmos. Sci.*, **54**, 2349-2361.

Hartmann, D.L. and F. Lo, 1998 : Wave-driven zonal flow vacillation in the Southern Hemisphere, *J. Atmos. Sci.*, **55**, 1303-1315.

Itoh, H., M. Kimoto and H. Aoki, 1999 : Alternation between the single and double jet structures in the Southern Hemisphere troposphere, *J. Meteor. Soc. Japan*, **77**, 399-412.

Lee, S. and S. Feldstein, 1996 : Mechanism of zonal index evolution in a two-layer model, *J. Atmos. Sci.*, **53**, 2232-2246.

Yoden, S., M. Shiotani and I. Hirota, 1987 : Multiple planetary flow regimes in the Southern Hemisphere, *J. Meteor. Soc. Japan*, **65**, 571-586.

Yu, J.-Y. and D.L. Hartmann, 1993 : Zonal flow vacillation and eddy forcing in a simple GCM of the atmosphere, *J. Atmos. Sci.*, **50**, 3244-3259.